AGU ADVANCING EARTH AND SPACE SCIENCE

Geophysical Research Letters

RESEARCH LETTER
10.1029/2021GL096030

Special Section:
Atmospheric Rivers: Intersection of Weather and Climate

Atmospheric Rivers Bring More Frequent and Intense Extreme Rainfall Events Over East Asia Under Global Warming

Y. Kamae[1], Y. Imada[2], H. Kawase[2], and W. Mei[3]

[1]Faculty of Life and Environmental Sciences, University of Tsukuba, Tsukuba, Japan, [2]Meteorological Research Institute, Japan Meteorological Agency, Tsukuba, Japan, [3]Department of Earth, Marine and Environmental Sciences, University of North Carolina at Chapel Hill, Chapel Hill, NC, USA

Key Points:

- Atmospheric rivers bring extreme rainfall over East Asia in current and future climates
- Atmospheric rivers are responsible for a large fraction of the increase in extreme rainfall over East Asia under global warming
- Intensified water vapor transports by atmospheric rivers cause record-breaking extreme rainfall events in a warmer climate

Supporting Information:

Supporting Information may be found in the online version of this article.

Correspondence to:

Y. Kamae,
kamae.yoichi.fw@u.tsukuba.ac.jp

Citation:

Kamae, Y., Imada, Y., Kawase, H., & Mei, W. (2021). Atmospheric rivers bring more frequent and intense extreme rainfall events over East Asia under global warming. *Geophysical Research Letters*, *48*, e2021GL096030. https://doi.org/10.1029/2021GL096030

Received 3 SEP 2021
Accepted 26 NOV 2021

Author Contributions:

Conceptualization: Y. Kamae
Data curation: Y. Kamae, Y. Imada, H. Kawase, W. Mei
Formal analysis: Y. Kamae
Funding acquisition: Y. Kamae
Investigation: Y. Kamae
Methodology: Y. Kamae, Y. Imada, H. Kawase, W. Mei
Project Administration: Y. Kamae, Y. Imada, H. Kawase

Abstract Portions of East Asia often experienced extremely heavy rainfall events over the last decade. Intense atmospheric rivers (ARs), eddy transports of moisture over the middle latitudes, contributed significantly to these events. Although previous studies pointed out that landfalling ARs will become more frequent under global warming, the extent to which ARs produce extreme rainfall over East Asia in a warmer climate remains unclear. Here we evaluate changes in the frequency and intensity of AR-related extreme heavy rainfall under global warming using a set of high-resolution global and regional atmospheric simulations. We find that both the AR-related water vapor transport and rainfall intensify over the southern and western slopes of mountains over East Asia in a warmer climate. ARs are responsible for a large fraction of the increase in the occurrence of extreme rainfall in boreal spring and summer. ARs will bring unprecedented extreme rainfall over East Asia under global warming.

Plain Language Summary In July 2018 and July 2020, East Asia suffered from extremely heavy rainfall events. The heavy rainfall was observed over a broad area because of organized water vapor flow associated with atmospheric rivers (ARs). ARs received increasing attention over the past decade because of such hazardous events. Under global warming, water vapor transports by ARs are enhanced. Using a set of global and regional atmospheric model simulations, we assessed the great role of ARs in the future extreme rainfall events. ARs with increased water vapor will bring record-breaking extreme rainfall when they make landfall over China, the Korean Peninsula and Japan. Such a great importance of ARs may also be found over other mid-latitude regions, including western North America and Europe.

1. Introduction

Atmospheric rivers, filamentary-shaped moisture transport bands, often bring heavy rainfall when they make landfall over the Northern and Southern Hemisphere middle latitudes (American Meteorological Society, 2019). AR-related heavy rainfall, heavy snowfall, and associated floods over the middle latitudes, especially during winter, have been a focus of many previous studies (e.g., Dettinger et al., 2011; Gimeno et al., 2016; Guan et al., 2010; Lavers et al., 2011; Massoud et al., 2020; Prince et al., 2021; Ralph et al., 2006). In recent years, people in East Asia frequently suffered from AR-related natural disasters (Hirota et al., 2016; Kamae, Mei, & Xie, 2017; Tsuji & Takayabu, 2019; Tsuji et al., 2020). Over East Asia, AR occurrence frequency peaks during warm seasons (i.e., spring, summer, and fall), in contrast to the seasonal variation in AR activity over the eastern North Pacific (Kamae, Mei, et al., 2017; Mundhenk et al., 2016; Pan & Lu, 2020). In April 2012, for example, an AR associated with an extratropical cyclone generated strong rainfall and record-breaking extreme winds over Japan (Figure S1 in Supporting Information S1). In July 2018 and July 2020, ARs passing through East Asia brought extreme rainfall and large social damages to the region (Araki et al., 2021; Hirockawa et al., 2020; Takemura et al., 2019; Tsuguti et al., 2019; Zhao et al., 2021). The higher frequency of AR-induced natural disasters in recent years suggest a possible influence of ongoing global warming on the occurrence of extreme events (e.g., Imada et al., 2020; Kamae, Shiogama, et al., 2017; Kawase et al., 2020, 2019).

Under global warming, changes in AR occurrence frequency and other properties (e.g., strength, size, and shape) may be attributed to thermodynamic and/or dynamic factors (e.g., Gao et al., 2015; Payne et al., 2020). Increased water vapor in the warmer air alone can lead to increased AR occurrence (Espinoza et al., 2018; Hagos et al., 2016; Lavers et al., 2013; Massoud et al., 2019). Over the western North Pacific, in addition to the thermodynamic

Resources: Y. Kamae, Y. Imada, H. Kawase, W. Mei
Software: Y. Kamae, W. Mei
Supervision: Y. Kamae
Validation: Y. Kamae, Y. Imada, H. Kawase, W. Mei
Visualization: Y. Kamae
Writing – original draft: Y. Kamae
Writing – review & editing: Y. Kamae, Y. Imada, H. Kawase, W. Mei

effect, dynamic effect associated with the changes in the western North Pacific Subtropical High (WNPSH) is also important for future changes in summertime AR activity (Kamae et al., 2019). The climate models participated in the Coupled Model Intercomparison Project Phase 5 (CMIP5) show divergent responses in the WNPSH under global warming (He & Zhou, 2015). If the WNPSH strengthens under global warming, more ARs are expected to occur over eastern China, the Korean Peninsula, and Japan in boreal summer, owing to enhanced moist southwesterly winds on the northwestern flank of the WNPSH (Kamae et al., 2019).

Previous studies have pointed out that global warming may lead to significant changes in the intensity and/or frequency of AR-related extreme rainfall over North America and Europe (Gao et al., 2016; Gershunov et al., 2019; Hagos et al., 2016; Radić et al., 2015; Warner et al., 2015). Most of these studies are based on global climate models with moderate horizontal (e.g., 0.75°–3.75°; Gao et al., 2016) and temporal (e.g., daily) resolutions, while higher spatial/temporal resolutions are more effective in evaluating changes in the characteristics of AR-related extreme rainfall. Huang et al. (2020) employed an ensemble downscaling experiments for western North America and identified significant changes in the intensity of AR-related extreme rainfall in a changing climate. In this study, we use high-resolution atmospheric general circulation model (AGCM) simulations and downscaling simulations by a regional climate model (RCM) to examine future change in AR-related rainfall over East Asia. The high-resolution RCM outputs (both in spatial and temporal) offer a great opportunity to evaluate the changes in orographic extreme rainfall associated with ARs.

2. Data and Methods

2.1. Current and Future Climate Simulations

We use a set of ensemble simulations with an AGCM and a RCM from the database for Policy Decision making for Future climate change (d4PDF, Ishii & Mori, 2020; Mizuta et al., 2017). The AGCM used in the d4PDF is the Meteorological Research Institute AGCM version 3.2 (MRI-AGCM3.2; Mizuta et al., 2012) with 60-km horizontal resolution and 64 vertical layers. This model realistically simulates rainfall (Ito et al., 2020) and AR activity (Kamae, Mei, et al., 2017) over East Asia. For the past simulations, the AGCM was driven by historical radiative forcing (greenhouse gases, aerosols, and ozone), sea surface temperature (SST) and sea ice (Hirahara et al., 2014) for 1951–2010 (PAST simulations hereafter). In addition to the PAST simulations, outputs from 60-year future simulations (PLUS4K simulations hereafter) were also examined to evaluate future change in extreme rainfall associated with ARs. In this set of simulations, the AGCM was driven by anomalous radiative forcing corresponding to the level of year 2090 in the Representative Concentration Pathway (RCP) 8.5, warmed SST and changes in sea ice. Six SST warming patterns obtained from CMIP5 multi-model results (Mizuta et al., 2014) were used to perform six-type PLUS4K simulations. The six SST warming patterns were based on RCP8.5 simulations by CCSM4, GFDL-CM3, HadGEM2-AO, MIROC5, MPI-ESM-MR, and MRI-CGCM3 (CC, GF, HA, MI, MP, and MR hereafter). The SST warming was scaled so that the simulated global-mean surface air temperature is 4 K warmer than the pre-industrial level (Mizuta et al., 2017). In this study, a 60-year climatology in the PAST and PLUS4K is compared to evaluate the effects of global warming on AR activity and extreme rainfall. Using the d4PDF AGCM output, Kamae et al. (2019) found an increase in AR frequency over East Asia under global warming. They also showed that the projected increase in AR activity is related to the patterns of tropical SST changes and the associated changes in WNPSH intensity. In the present study, we further evaluate AR contributions to extreme rainfall using output from the downscaling simulations described below.

The d4PDF also provides outputs from regional downscaling simulations covering Japan, the Korean Peninsula and eastern China (Figure S2a in Supporting Information S1). The d4PDF RCM simulations were performed by the Nonhydrostatic Regional Climate Model (NHRCM; Sasaki et al., 2008) with 20-km grid spacing and 40 vertical layers (Mizuta et al., 2017). Model outputs at every one hour with 20-km horizontal resolution are more instrumental in examining extreme rainfall than the 6-hr outputs from the d4PDF AGCM simulations with a 60-km horizontal resolution. The combination of the d4PDF AGCM and RCM simulations greatly facilitates the evaluation of the changes in extreme rainfall associated with ARs under climate change (Fujita et al., 2019; Imada et al., 2020; Kawase et al., 2019, 2020; Miyasaka et al., 2020). In this study, we defined extreme rainfall events in the PAST simulations as upper 0.1% cases of wet hours (rainfall >0.1 mm hr^{-1}) using 1-hr outputs of the RCM simulations. This threshold obtained from the PAST simulations was also used to define extreme rainfall events in the PLUS4K simulations and evaluate changes in frequency of events under global warming (see Figure 1c of Schär et al., 2016). We calculated a 60-year climatology for each simulation, then averaged across ensemble

members (10 members for PAST and 30 members for PLUS4K simulations; 5 members for each of the six-type PLUS4K simulations) to minimize the effects of atmospheric internal variability (Kamae, Mei, et al., 2017; Kamae, Shiogama, et al., 2017).

2.2. AR Detection

Using outputs from the d4PDF AGCM runs, ARs were detected at 6-hr intervals based on vertically integrated water vapor transport (IVT) as calculated below:-

$$\mathrm{IVT} = \sqrt{\left(-\frac{1}{g}\int_{1000}^{300} qu \; dp\right)^2 + \left(-\frac{1}{g}\int_{1000}^{300} qv \; dp\right)^2} \quad (1)$$

where q is specific humidity, u is zonal wind, v is meridional wind, p is air pressure, and g is the acceleration due to gravity. ARs were detected using IVT field following the method described in Kamae, Mei, et al. (2017), which is modified from the method proposed in Mundhenk et al. (2016). Anomalous IVT in the PAST simulations was obtained by comparing with its daily climatology. For the PLUS4K simulations, daily climatology in the PLUS4K simulations was subtracted to obtain IVT anomaly (Kamae et al., 2019, 2021). ARs were detected based on shapes (length >1,500 km, area $>7.8 \times 10^5$ km^2, length-width ratio >1.325) and intensity (140 kg m^{-1} s^{-1}) of the anomalous IVT. Kamae, Mei, et al. (2017) showed that the climatology and interannual variability of AR occurrence frequency in the d4PDF AGCM simulations are generally consistent with those in observations. Details on future change in the frequency of the detected ARs in the d4PDF AGCM simulations can be found in Kamae et al. (2019, 2021).

We compared the AR data obtained from the AGCM runs with rainfall simulated in the RCM runs to evaluate AR-related rainfall and its extremes. The 6-hr, 60-km resolution data of AGCM-based AR were linearly interpolated to the 1-hr, 20 km-resolution. We confirmed that the positions of the detected ARs in the AGCM runs are generally consistent with those in the RCM runs (Figure S3 in Supporting Information S1).

3. Results

3.1. Climatology of AR Rainfall and Its Change Under Global Warming

Figure 1 shows the climatology of AR-related rainfall for individual seasons. As shown in Kamae, Mei, and Xie (2017), AR-related rainfall pattern manifests a strong orographic effect. Peaks in AR-related rainfall are found on the southern and western slopes of mountains over East Asia (western Japan, central Japan, northern Japan, Taiwan, the Korean Peninsula, and northeastern China). In particular, AR rainfall dominates at the southwestern slope of Japan's Alps (Figure S2b in Supporting Information S1) in all seasons, therefore we focus on this region in the latter part of this study. The spatial pattern of AR rainfall climatology in the simulations is similar to that obtained from observations and an atmospheric reanalysis (Kamae, Mei, & Xie, 2017), indicating that the AR–rainfall relationship over East Asia is well reproduced in the AGCM/RCM. Table 1 summarizes the climatology of AR-related rainfall averaged over the "southern-western slope" regions over East Asia (Figure S2b in Supporting Information S1). ARs produce rainfall of 22.8–27.4 mm day^{-1} on average, contributing to a large fraction of total rainfall in these regions (Figure S4 in Supporting Information S1). Table 1 also summarizes AR fraction in the occurrence of extreme rainfall (Section 2.1). The relative fraction is highest in MAM (67.7%) and relatively lower in JJA and SON (41.7% and 49.2%, respectively). This seasonal variation is also found in observations and can be interpreted as a result of the dominance of Meiyu-Baiu rainband and tropical cyclones in JJA and SON (Kamae, Mei, & Xie, 2017).

Before examining change in AR-related rainfall under global warming, we compare the past and future climatology of AR occurrence frequency. Black contours in Figure 2 show the seasonal-mean climatology of AR frequency over the western North Pacific. In the PAST simulations, ARs are most active during JJA (Figure 2b), particularly over the Pacific coast of Japan (Kamae, Mei, et al., 2017). No ARs are detected over western China in DJF, owing to sparce moisture in the air (Figures 3a and 3d in Kamae, Mei, et al., 2017). As examined in Kamae et al. (2019), East-Asian ARs become more frequent in a warmer climate. During MAM, for example, low-level westerly is enhanced over the middle latitudes (the area between anomalous subtropical high pressure and subpolar low pressure; Figure 1c of Kamae et al., 2019) and AR frequency increases (shading in Figure 2a) over southeastern

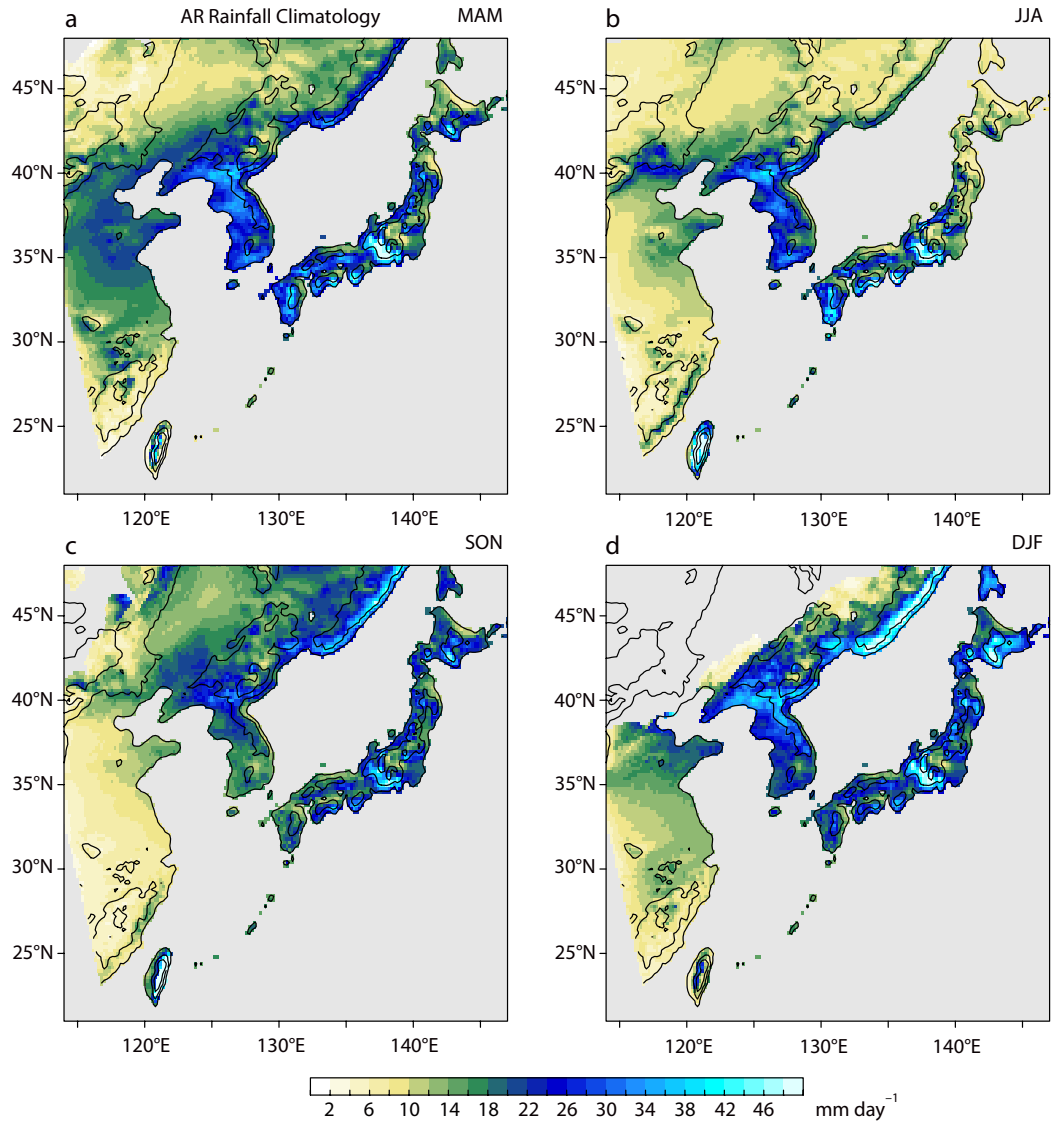

Figure 1. Climatology of atmospheric river (AR)-related rainfall over East Asia. Rainfall (mm day^{-1}) accompanied with ARs are averaged for 1951–2010 in the d4PDF RCM ensemble simulations for (a) March-April-May (MAM), (b) June-July-August (JJA), (c) September-October-November (SON), and (d) December-January-February (DJF). Gray shading indicates areas with no ARs or ocean area or area outside of the RCM simulation (see Figure S2 in Supporting Information S1). Contours indicate topography of 400 and 1,200 m.

Table 1
Climatology in AR-Related Rainfall

	MAM	JJA	SON	DJF
Climatology in AR Rainfall (mm day^{-1})	27.4 ± 0.5	25.2 ± 0.5	22.8 ± 0.7	26.4 ± 1.2
AR Fraction in Extreme Rainfall (%)	67.7 ± 0.8	41.7 ± 1.0	49.2 ± 2.8	50.5 ± 2.9

Note. Top and bottom rows indicate climatology in AR-related rainfall (mm day^{-1}) and fraction (%) of occurrence frequency of AR-related extreme rainfall (f_AR$_p$) to that of all extreme rainfall (f$_p$) in the PAST simulations for each season averaged over "southern-western slope" regions over East Asia (Figure S2b in Supporting Information S1). Extreme rainfall events are defined as upper 0.1% cases of wet hours (rainfall >0.1 mm hr^{-1}). Uncertainty ranges indicate 95% confidence intervals.

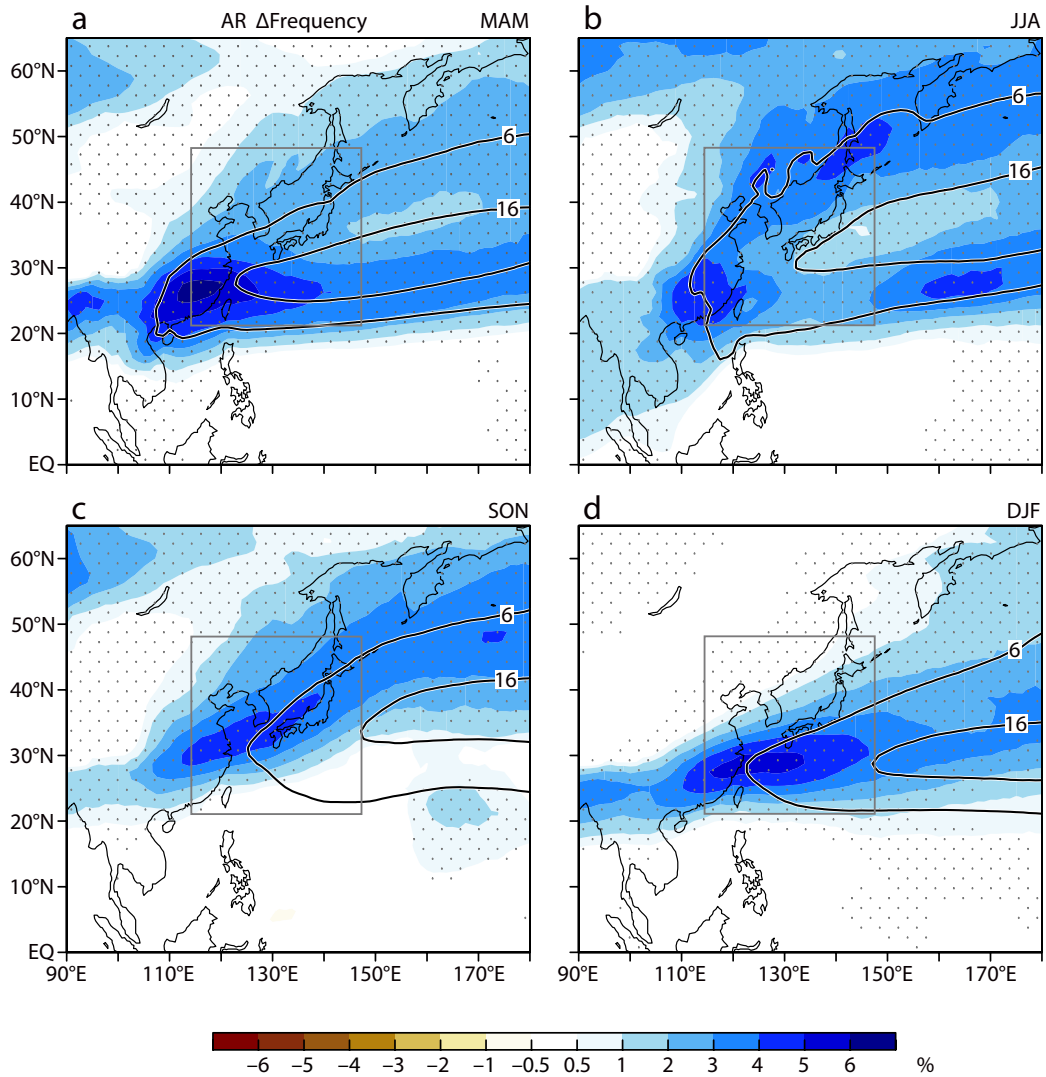

Figure 2. Ensemble mean changes in occurrence frequency of atmospheric rivers (ARs) between the PLUS4K and PAST simulations. The change in frequency of ARs (ΔARs) is derived from the d4PDF AGCM simulations (PLUS4K minus PAST) for (a) March-April-May (MAM), (b) June-July-August (JJA), (c) September-October-November (SON), and (d) December-January-February (DJF). Stipples indicate the areas with 95% statistical confidence in ΔARs. Contours indicate 6% and 16% of climatology in AR frequency in the PAST simulations. Gray rectangle indicates the analysis area shown in Figure 1.

China (+3–6%), Korean Peninsula (+2–3%), Japan (+2–4%) and northeastern China (+1–3%). The increase is found among all six-type global warming simulations, suggesting a significant and robust increase in occurrence of AR-related rainfall over East Asia.

In the d4PDF simulations, East-Asian extreme rainfall becomes more frequent and intense under global warming, as demonstrated in previous studies (e.g., Endo et al., 2017; Fujita et al., 2019). Seasonal-mean changes in frequency of extreme rainfall (PLUS4K minus PAST) averaged over the "southern-western slope" regions are larger during MAM and DJF than JJA and SON (Table S1 in Supporting Information S1). The changes in frequency during JJA and SON over East Asia (Figure S5 in Supporting Information S1) are significantly influenced by tropical cyclone activity, as demonstrated in Endo et al. (2017). In MAM, the frequency of extreme rainfall triples (+206 ± 11%) with non-negligible spread among simulations with different SST warming patterns (for example, +159% in CC, +244% in MI). The spread may be attributed to the differences in the dynamic atmospheric circulation (Pfahl et al., 2017), which in turn are associated with the differences in SST warming pattern (Figure S6 in Supporting Information S1). Kamae et al. (2019) revealed that the spread in East-Asian atmospheric circulation

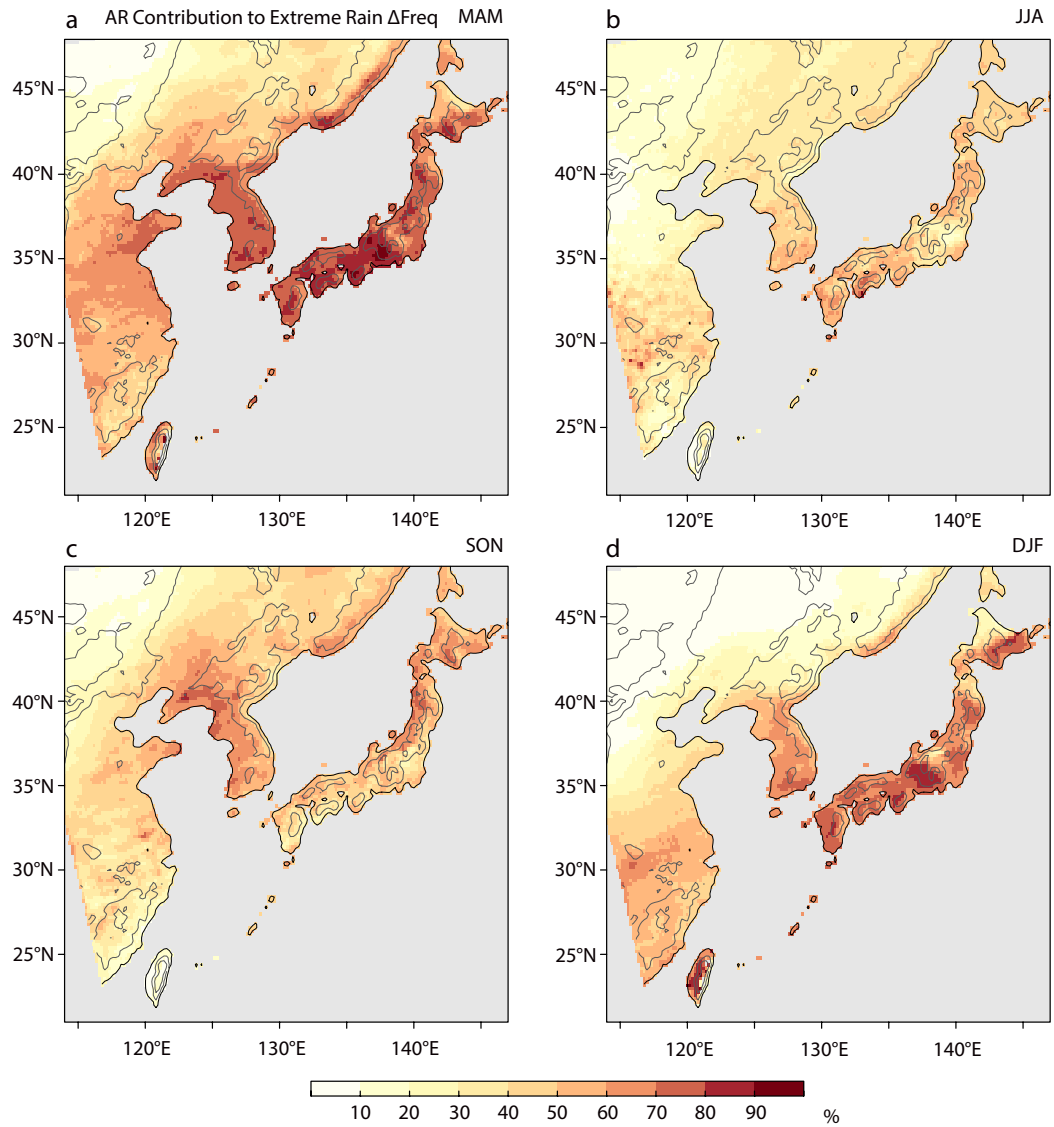

Figure 3. Ensemble mean atmospheric river (AR) contributions to the changes in occurrence frequency of extreme rainfall. Each panel show the ratio (%), represented as $100(f\_AR_{P4}–f\_AR_P)/(f_{P4}–f_P)$ for (a) MAM, (b) JJA, (c) SON, and (d) December-January-February (DJF), where f_P is occurrence frequency of extreme rainfall in the PAST simulation, f_{P4} is that of the PLUS4K simulation (see Figure S5 in Supporting Information S1), f_AR_P and f_AR_{P4} are those of AR-related extreme rainfall in the PAST and PLUS4K simulations, respectively.

response to SST warming in the d4PDF simulations (0.70%–1.14% per 1 K of tropical-mean SST warming) is primarily related to the warming patterns over the Indian and Pacific Oceans.

It is expected that ARs play an important role in increasing the occurrence of extreme rainfall under global warming. Figure 3 shows the contributions of ARs to the increase in the occurrence of extreme rainfall. ARs contribute greatly to the large increase in extreme rainfall, especially in MAM and DJF. Prominent differences exist in the spatial pattern of the contributions (for example, between western and eastern Kyushu, and between south-west slope and east slope of the Japan's Alps), indicating a strong orographic effect on AR-related extreme rainfall. Table 2 summarizes the averaged contributions over the "southern-western slope" regions. ARs explain 76.6 ± 0.6% of the increase in the occurrence of extreme rainfall during MAM. The AR contribution becomes lower in JJA and SON (46.2 ± 0.9% and 55.4 ± 1.1%, respectively), largely owing to the significant contributions of Meiyu-Baiu rainband and tropical cyclones (Endo et al., 2017). The spread in AR contributions among

Table 2
AR Contribution to the Change in Occurrence Frequency of Extreme Rainfall for Each Season Averaged Over the "Southern-Western Slope" Regions in Each Simulation

AR contribution to increase in extreme rainfall (%)	MAM	JJA	SON	DJF
All	76.6 ± 0.6	46.2 ± 0.9	55.4 ± 1.1	64.9 ± 1.7
CC	78.0 ± 4.4	43.5 ± 5.2	55.3 ± 3.0	65.6 ± 10.7
GF	74.2 ± 3.9	43.6 ± 3.0	52.0 ± 4.5	63.7 ± 3.2
HA	77.6 ± 1.9	48.0 ± 5.9	52.4 ± 6.7	69.5 ± 4.4
MI	76.9 ± 3.1	50.4 ± 16.1	54.7 ± 8.6	58.4 ± 6.2
MP	77.8 ± 1.6	44.0 ± 3.7	61.0 ± 4.6	61.1 ± 3.7
MR	74.8 ± 2.8	47.4 ± 5.9	56.7 ± 4.5	71.0 ± 7.0

Note. The ratio (%) is represented as $100(f\_AR_{P4}–f\_AR_P)/(f_{P4}–f_P)$ as shown in Figure 3. "All" indicates ensemble mean of the six simulations. Uncertainty ranges indicate 95% confidence intervals.

the six-type warming simulations is modest (for example, 74.2%–78.0% in MAM and 43.5%–50.4% in JJA), suggesting the robust AR contributions to the increasing occurrence of extreme rainfall.

3.2. Water Vapor Transport and Rainfall

Landfalling ARs bring large-scale water vapor flow to East Asia and cause heavy rainfall in the region. Under global warming, strengthened water vapor transport combined with orographic uplift over steep mountains should result in more intense local rainfall. In this subsection, we examine the relationship between the large-scale IVT simulated in the AGCM and the local rainfall resolved in the RCM. Figure 4 shows the joint probability distribution of IVT and rainfall over the southwestern slope of Japan's Alps (Figure S2b in Supporting Information S1) in MAM. We chose this region as a representative of the regions with strong AR-related orographic rainfall (Figures 1 and 3; and Figure S3 in Supporting Information S1). In the PAST simulations (Figure 4a), the largest probability is found in IVT cases weaker than 200 kg m^{-1} s^{-1} (horizontal axis) with rainfall less than 1 mm hr^{-1} (vertical axis), and stronger IVT cases have a larger chance of producing heavy rainfall. For example, IVT of 400 kg m^{-1} s^{-1} have a 0.01% chance of generating rainfall of around 9 mm hr^{-1}, whereas the chance is 0.001% for IVTs of 150 kg m^{-1} s^{-1}. This IVT–rainfall relationship is tied to the strong orographic effect over the southwestern slope of Japan's Alps (Kamae, Mei, & Xie, 2017). In the PAST simulations, the upper-end of IVT and rainfall are 1200 kg m^{-1} s^{-1} and 29 mm hr^{-1}, respectively.

Under global warming, both the IVT and rainfall are enhanced over this region. Figure 4b shows the IVT–rainfall relationship in the PLUS4K simulations. The probability distribution generally shifts toward stronger sides of IVT and rainfall compared to the PAST simulations. From this panel, we can also identify extreme IVT or rainfall in a warmer climate above the upper-end level in the PAST simulations (i.e., IVT >1200 kg m^{-1} s^{-1} and rainfall >29 mm hr^{-1}; Figure 4a). If we limit to AR-related cases, these probability distributions are only found in stronger IVT bins, in line with the definition of ARs (Figure S7 in Supporting Information S1). Over central Japan, AR fraction in each bin shown in Figure 4c clearly demonstrates a great importance of ARs in increasing extreme rainfall in a warmer climate. As summarized in Table 2, 76.6% of increased extreme rainfall under global warming over the "southern-western slope" regions in MAM are associated with ARs. The occurrence of

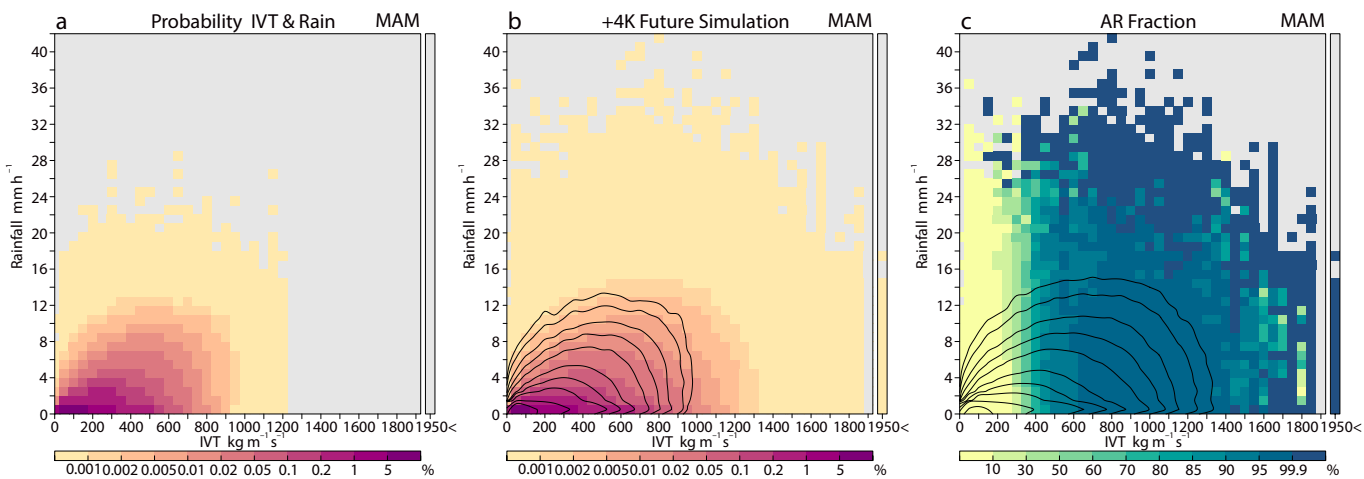

Figure 4. Joint PDF on the rainfall–IVT plane. The PDF is obtained from rainfall at the southwestern slope of Japan's Alps (137.3°–137.7°E, 35.7°–36.3°N and 137.7°–138.1°E, 35.3°–35.9°N) in the d4PDF RCM simulations and IVT (136.9°–138.1°E, 35.6°–36.9°N) in the d4PDF AGCM simulations; (see Figure S2 in Supporting Information S1) in MAM. (a) The PAST and (b) PLUS4K simulations. Contours in (b) indicate probability shown in (a). (c) Fraction of AR-related events at each bin in the PLUS4K simulation. Contours in (c) indicate probability shown in (b).

extreme rainfall stronger than 29 mm hr^{-1} in the PLUS4K simulations, not occurred in the PAST simulation, is due primarily to ARs (89.3%).

4. Summary and Discussion

The ensemble simulations based on the AGCM and RCM indicate that more ARs pass through East Asia in a warmer climate. In the future simulations, ARs often bring more water vapor and more intense rainfall over the southern and western slopes of mountains over western Japan, central Japan, northern Japan, Taiwan, the Korean Peninsula, and northeastern mainland China, compared to the PAST simulations. The increase in the occurrence frequency of AR-related extreme rainfall peaks in MAM because of the contributions of other phenomena (including tropical cyclones) to extreme rainfall in JJA and SON. The results of this study indicate that more record-breaking intense rainfall events will occur in a warmer climate and are greatly contributed by ARs.

In this study, we focus on rainfall over East Asia, because of the limitation in computational resources in integrating both the AGCM and RCM for past and future ensemble simulations. However, the findings of this study should also apply to other mid-latitude regions. Over western North America or Europe, for example, landfalling ARs often bring heavy rainfall when they encontour the steep mountains. The AR-related orographic rainfall should be intensified in a warmer climate because of increased water vapor transport (e.g., Gao et al., 2016; Gershunov et al., 2019; Hagos et al., 2016; Huang et al., 2020; Radić et al., 2015; Warner et al., 2015). Note that the uncertainty in the future changes of AR activity and of AR contributions to extreme rainfall are not necessarily fully covered by the ensemble simulations with a single AGCM. Also, the presented results may partly depend on the algorithm of AR detection (Ryu et al., 2021; Shields et al., 2018). Further studies using multiple climate model outputs and different detection algorithms are needed to evaluate the robustness of the future changes in AR frequency, AR intensity, and AR-related extreme rainfall.

Data Availability Statement

All the data used for the analyses in this study are available via DIAS repository (http://search.diasjp.net/en/dataset/d4PDF_GCM and http://search.diasjp.net/en/dataset/d4PDF_RCM).

Acknowledgments
We thank two anonymous reviewers for their constructive comments. We would like to acknowledge I. Takayabu for providing helpful comments and suggestions. This work was supported by JSPS KAKENHI Grant Numbers 19H05704, 19H05703, and 19H05697 and the Integrated Research Program for Advancing Climate Models (TOUGOU) Grant Numbers JPMXD0717935457 and JPMXD0717935561 from the Ministry of Education, Culture, Sports, Science and Technology (MEXT), Japan. The Earth Simulator was used for the d4PDF ensemble simulation as "Strategic Project with Special Support" of JAMSTEC.

References

American Meteorological Society. (2019). *Atmospheric River*. Retrieved from http://glossary.ametsoc.org/wiki/Atmospheric_river

Araki, K., Kato, T., Hirockawa, Y., & Mashiko, W. (2021). Characteristics of atmospheric environments of quasi-stationary convective bands in Kyushu, Japan during the July 2020 heavy rainfall event. *SOLA*, *17*, 8–15. https://doi.org/10.2151/sola.2021-002

Dettinger, M. D., Ralph, F. M., Das, T., Neiman, P. J., & Cayan, D. R. (2011). Atmospheric rivers, floods, and the water resources of California. *Water*, *3*(2), 445–478. https://doi.org/10.3390/w3020445

Endo, H., Kitoh, A., Mizuta, R., & Ishii, M. (2017). Future changes in precipitation extremes in East Asia and their uncertainty based on large ensemble simulations with a high-resolution AGCM. *SOLA*, *13*, 7–12. https://doi.org/10.2151/sola.2017-002

Espinoza, V., Waliser, D. E., Guan, B., Lavers, D. A., & Ralph, F. M. (2018). Global analysis of climate change projection effects on atmospheric rivers. *Geophysical Research Letters*, *45*(9), 4299–4308. https://doi.org/10.1029/2017GL076968

Fujita, M., Mizuta, T., Ishii, M., Endo, H., Sato, T., Okada, Y., et al. (2019). Precipitation changes in a climate with 2-K surface warming from large ensemble simulations using 60-km global and 20-km regional atmospheric models. *Geophysical Research Letters*, *46*(1), 435–442. https://doi.org/10.1029/2018GL079885

Gao, Y., Lu, J., & Leung, L. R. (2016). Uncertainties in projecting future changes in atmospheric rivers and their impacts on heavy precipitation over Europe. *Journal of Climate*, *29*(18), 6711–6726. https://doi.org/10.1175/JCLI-D-16-0088.1

Gao, Y., Lu, J., Leung, L. R., Yang, Q., Hagos, S., & Qian, Y. (2015). Dynamical and thermodynamical modulations on future changes of landfalling atmospheric rivers over western North America. *Geophysical Research Letters*, *42*(17), 7179–7186. https://doi.org/10.1002/2015GL065435

Gershunov, A., Shulgina, T., Clemesha, R. E. S., Guirguis, K., Pierce, D. W., Dettinger, M. D., et al. (2019). Precipitation regime change in Western North America: The role of atmospheric rivers. *Scientific Reports*, *9*, 9944. https://doi.org/10.1038/s41598-019-46169-w

Gimeno, L., Dominguez, F., Nieto, R., Trigo, R., Drumond, A., Reason, C. J. C., et al. (2016). Major mechanisms of atmospheric moisture transport and their role in extreme precipitation events. *Annual Review of Environment and Resources*, *41*, 117–141. https://doi.org/10.1146/annurev-environ-110615-085558

Guan, B., Molotch, N. P., Waliser, D. E., Fetzer, E. J., & Neiman, P. J. (2010). Extreme snowfall events linked to atmospheric rivers and surface air temperaturevia satellite measurements. *Geophysical Research Letters*, *37*(20), L20401. https://doi.org/10.1029/2010GL044696

Hagos, S. M., Leung, L. R., Yoon, J.-H., Lu, J., & Gao, Y. (2016). A projection of changes in landfalling atmospheric river frequency and extreme precipitation over western North America from the Large Ensemble CESM simulations. *Geophysical Research Letters*, *43*(3), 1357–1363. https://doi.org/10.1002/2015gl067392

He, C., & Zhou, T. (2015). Responses of the western North Pacific subtropical high to global warming under RCP4.5 and RCP8.5 scenarios projected by 33 CMIP5 models: The dominance of tropical Indian Ocean–tropical western Pacific SST gradient. *Journal of Climate*, *28*(1), 365–380. https://doi.org/10.1175/JCLI-D-13-00494.1

Hirahara, S., Ishii, M., & Fukuda, Y. (2014). Centennial-scale sea surface temperature analysis and its uncertainty. *Journal of Climate*, *27*(1), 57–75. https://doi.org/10.1175/JCLI-D-12-00837.1

Hirockawa, Y., Kato, T., Araki, K., & Mashiko, W. (2020). Characteristics of an extreme rainfall event in Kyushu district, southwestern Japan in early July 2020. *SOLA*, *16*, 265–270. https://doi.org/10.2151/sola.2020-044

Hirota, N., Takayabu, Y. N., Kato, M., & Arakane, S. (2016). Roles of an atmospheric river and a cutoff low in the extreme precipitation event in Hiroshima on 19 August 2014. *Monthly Weather Review*, *144*(3), 1145–1160. https://doi.org/10.1175/MWR-D-15-0299.1

Huang, X., Swain, D. L., & Hall, A. D. (2020). Future precipitation increase from very high resolution ensemble downscaling of extreme atmospheric river storms in California. *Science Advances*, *6*(29), eaba1323. https://doi.org/10.1126/sciadv.aba1323

Imada, Y., Kawase, H., Watanabe, M., Arai, M., Shiogama, H., & Takayabu, I. (2020). Advanced risk-based event attribution for heavy regional rainfall events. *npj Climate and Atmospheric Science*, *3*, 37. https://doi.org/10.1038/s41612-020-00141-y

Ishii, M., & Mori, N. (2020). d4PDF: Large-ensemble and high-resolution climate simulations for global warming risk assessment. *Progress in Earth and Planetary Science*, *7*, 58. https://doi.org/10.1186/s40645-020-00367-7

Ito, R., Nakaegawa, T., & Takayabu, I. (2020). Comparison of regional characteristics of land precipitation climatology projected by an MRI-AGCM multi-cumulus scheme and multi-SST ensemble with CMIP5 multi-model ensemble projections. *Progress in Earth and Planetary Science*, *7*, 77. https://doi.org/10.1186/s40645-020-00394-4

Kamae, Y., Mei, W., & Xie, S.-P. (2017). Climatological relationship between warm season atmospheric rivers and heavy rainfall over East Asia. *Journal of the Meteorological Society of Japan*, *95*(6), 411–431. https://doi.org/10.2151/jmsj.2017-027

Kamae, Y., Mei, W., & Xie, S.-P. (2019). Ocean warming pattern effects on future changes in East Asian atmospheric rivers. *Envrionmental Research Letters*, *14*, 054019. https://doi.org/10.1088/1748-9326/ab128a

Kamae, Y., Mei, W., & Xie, S.-P. (2021). Corrigendum: Ocean warming pattern effects on future changes in East Asian atmospheric rivers (2019). *Environmental Research Letters*, *16*(9), 099501. https://doi.org/10.1088/1748-9326/ac1700

Kamae, Y., Mei, W., Xie, S.-P., Naoi, M., & Ueda, H. (2017). Atmospheric rivers over the Northwestern Pacific: Climatology and interannual variability. *Journal of Climate*, *30*(15), 5605–5619. https://doi.org/10.1175/JCLI-D-16-0875.1

Kamae, Y., Shiogama, H., Imada, Y., Mori, M., Arakawa, O., Mizuta, R., et al. (2017). Forced response and internal variability of summer climate over western North America. *Climate Dynamics*, *49*(1–2), 403–417. https://doi.org/10.1007/s00382-016-3350-x

Kawase, H., Imada, Y., Sasaki, H., Nakaegawa, T., Murata, A., Nosaka, M., & Takayabu, I. (2019). Contribution of historical global warming to local-scale heavy precipitation in western Japan estimated by large ensemble high-resolution simulations. *Journal of Geophysical Research: Atmospheres*, *124*(12), 6093–6103. https://doi.org/10.1029/2018JD030155

Kawase, H., Imada, Y., Tsuguti, H., Nakaegawa, T., Seino, N., Murata, A., & Takayabu, I. (2020). The heavy rain event of July 2018 in Japan enhanced by historical warming. *Bullten of American Meteorological Society*, *101*(1), S109–S114. https://doi.org/10.1175/BAMS-D-19-0173.1

Lavers, D. A., Allan, R. P., Villarini, G., Lloyd-Hughes, B., Brayshaw, D. J., & Wade, A. J. (2013). Future changes in atmospheric rivers and their implications for winter flooding in Britain. *Envrionmental Research Letters*, *8*, 034010. https://doi.org/10.1088/1748-9326/8/3/034010

Lavers, D. A., Allan, R. P., Wood, E. F., Villarini, G., Brayshaw, D. J., & Wade, A. J. (2011). Winter floods in Britain are connected to atmospheric rivers. *Geophysical Research Letters*, *38*(23), L23803. https://doi.org/10.1029/2011GL049783

Massoud, E., Massoud, T., Guan, B., Sengupta, A., Espinoza, V., De Luna, M., et al. (2020). Atmospheric rivers and precipitation in the Middle East and North Africa (MENA). *Water*, *12*(10), 2863. https://doi.org/10.3390/w12102863

Massoud, E. C., Espinoza, V., Guan, B., & Waliser, D. E. (2019). Global climate model ensemble approaches for future projections of atmospheric rivers. *Earth's Future*, *7*(10), 1136–1151. https://doi.org/10.1029/2019EF001249

Miyasaka, T., Kawase, H., Nakaegawa, T., Imada, Y., & Takayabu, I. (2020). Future projections of heavy precipitation in Kanto and associated weather patterns using large ensemble high-resolution simulations. *SOLA*, *16*, 125–131. https://doi.org/10.2151/sola.2020-022

Mizuta, R., Arakawa, O., Ose, T., Kusunoki, S., Endo, H., & Kitoh, A. (2014). Classification of CMIP5 future climate responses by the tropical sea surface temperature changes. *SOLA*, *10*, 167–171. https://doi.org/10.2151/sola.2014-035

Mizuta, R., Murata, A., Ishii, M., Shiogama, H., Hibino, K., Mori, N., et al. (2017). Over 5000 years of ensemble future climate simulations by 60-km global and 20-km regional atmospheric models. *Bullten of American Meteorological Society*, *98*(7), 1383–1398. https://doi.org/10.1175/BAMS-D-16-0099.1

Mizuta, R., Yoshimura, H., Murakami, H., Matsueda, M., Endo, H., Ose, T., et al. (2012). Climate simulations using MRI-AGCM3.2 with 20-km grid. *Journal of the Meteorological Society of Japan*, *90A*, 233–258. https://doi.org/10.2151/jmsj.2012-A12

Mundhenk, B. D., Barnes, E. A., & Maloney, E. D. (2016). All-season climatology and variability of atmospheric river frequencies over the North Pacific. *Journal of Climate*, *29*(13), 4885–4903. https://doi.org/10.1175/JCLI-D-15-0655.1

Pan, M., & Lu, M. (2020). East Asia atmospheric river catalog: Annual cycle, transition mechanism, and precipitation. *Geophysical Research Letters*, *47*(15), e2020GL089477. https://doi.org/10.1029/2020GL089477

Payne, A. E., Demory, M.-E., Leung, L. R., Ramos, A. M., Shields, C. A., Rutz, J. J., et al. (2020). Responses and impacts of atmospheric rivers to climate change. *Nature Reviews Earth & Environment*, *1*, 143–157. https://doi.org/10.1038/s43017-020-0030-5

Pfahl, S., O'Gorman, P. A., & Fischer, E. M. (2017). Understanding the regional pattern of projected future changes in extreme precipitation. *Nature Climate Change*, *7*, 423–427. https://doi.org/10.1038/nclimate3287

Prince, H. D., Cullen, N. J., Gibson, P. B., Conway, J., & Kingston, D. G. (2021). A climatology of atmospheric rivers in New Zealand. *Journal of Climate*, *34*, 4383–4402. https://doi.org/10.1175/JCLI-D-20-0664.1

Radić, V., Cannon, A. J., Menounos, B., & Gi, N. (2015). Future changes in autumn atmospheric river events in British Columbia, Canada, as projected by CMIP5 global climate models. *Journal of Geophysical Research: Atmosphere*, *120*(18), 9279–9302. https://doi.org/10.1002/2015JD023279

Ralph, F. M., Neiman, P. J., Wick, G. A., Gutman, S. I., Dettinger, M. D., Cayan, D. R., & White, A. B. (2006). Flooding on California's Russian River: Role of atmospheric rivers. *Geophysical Research Letters*, *33*, L13801. https://doi.org/10.1029/2006GL026689

Ryu, Y., Moon, H., Kim, J., Kim, T.-J., Boo, K.-O., Guan, B., et al. (2021). A multi-inventory ensemble analysis of the effects of atmospheric rivers on precipitation and streamflow in the Namgang-dam inflow basin in Korea. *Water Resources Research*, *57*, e2021WR030058. https://doi.org/10.1029/2021WR030058

Sasaki, H., Kurihara, K., Takayabu, I., & Uchiyama, T. (2008). Preliminary experiments of reproducing the present climate using the nonhydrostatic regional climate model. *SOLA*, *4*, 25–28. https://doi.org/10.2151/sola.2008-007

Schär, C., Ban, N., Fischer, E. M., Rajczak, J., Schmidli, J., Frei, C., et al. (2016). Percentile indices for assessing changes in heavy precipitation events. *Climatic Change*, *137*(1), 201–216. https://doi.org/10.1007/s10584-016-1669-2

Shields, C. A., Rutz, J. J., Leung, L.-Y., Ralph, F. M., Wehner, M., Kawzenuk, B., et al. (2018). Atmospheric river tracking method intercomparison project (ARTMIP): Project goals and experimental design. *Geoscientific Model Development*, *11*(6), 2455–2474. https://doi.org/10.5194/gmd-11-2455-2018

Takemura, K., Wakamatsu, S., Togawa, H., Shimpo, A., Kobayashi, C., Maeda, S., & Nakamura, H. (2019). Extreme moisture flux convergence over western Japan during the heavy rain event of July 2018. *SOLA*, *15A*, 49–54. https://doi.org/10.2151/sola.15A-009

Tsuguti, H., Seino, N., Kawase, H., Imada, Y., Nakaegawa, T., & Takayabu, I. (2019). Meteorological overview and mesoscale characteristics of the heavy rain event of July 2018 in Japan. *Landslides*, *16*, 363–371. https://doi.org/10.1007/s10346-018-1098-6

Tsuji, H., & Takayabu, Y. N. (2019). Precipitation enhancement via the interplay between atmospheric rivers and cutoff lows. *Monthly Weather Review*, *147*(7), 2451–2466. https://doi.org/10.1175/MWR-D-18-0358.1

Tsuji, H., Yokoyama, C., & Takayabu, Y. N. (2020). Contrasting features of the July 2018 heavy rainfall event and the 2017 northern Kyushu rainfall event in Japan. *Journal of the Meteorological Society of Japan*, *98*(4), 859–876. https://doi.org/10.2151/jmsj.2020-045

Warner, M. D., Mass, C. F., & Salathé, E. P., Jr. (2015). Changes in winter atmospheric rivers along the North American West Coast in CMIP5 climate models. *Journal of Hydrometeorology*, *16*(1), 118–128. https://doi.org/10.1175/JHM-D-14-0080.1

Zhao, N., Manda, A., Guo, X., Kikuchi, K., Nasuno, T., Nakano, M., et al. (2021). A Lagrangian view of moisture transport related to the heavy rainfall of July 2020 in Japan: Importance of the moistening over the subtropical regions. *Geophysical Research Letters*, *48*(5), e2020GL091441. https://doi.org/10.1029/2020GL091441

References From the Supporting Information

Kamiguchi, K., Arakawa, O., Kitoh, A., Yatagai, A., Hamada, A., & Yasutomi, N. (2010). Development of APHRO_JP, the first Japanese high-resolution daily precipitation product for more than 100 years. *Hydrological Research Letters*, *4*, 60–64. https://doi.org/10.3178/hrl.4.60

Kobayashi, S., Ota, Y., Harada, Y., Ebita, A., Moriya, M., Onda, H., et al. (2015). The JRA-55 Reanalysis: General specifications and basic characteristics. *Journal of the Meteorological Society of Japan*, *93*(1), 5–48. https://doi.org/10.2151/jmsj.2015-001